# METEOROID'S ORBIT DETERMINATION

SIMON ANGHEL[1,3,4,*], IHARKA SZÜCS-CSILLIK[2,*], DAN-ALIN NEDELCU[1,3], IOANA BOACA[1], MIREL BIRLAN[3,1]

[1] *Romanian Academy, Astronomical Institute Ro-40557, Cuţitul de Argint 5, Bucharest, Romania*
*Email: simonanghel@gmail.com*

[2] *Romanian Academy, Astronomical Institute Astronomical Observatory of Cluj-Napoca Ro-400487, Cireşilor 19, Cluj-Napoca, Romania*

[3] *Institut de Mécanique Céleste et de Calculs des Éphémérides, CNRS UMR 8028, Observatoire de Paris, PSL Research University, 77 Av. Denfert-Rochereau, 75014 Paris Cedex, France*

[4] *Faculty of Physics, University of Bucharest 405-Atomistilor, 077125 Magurele, Ilfov, Romania*

*Abstract.* The expanding of meteor networks has allowed an ever increasing precision in trajectory computations. This translates into a better constraining of the state vector, and by integration, the orbital torus along which the parent body can be found. Here, we present a theoretical method of orbit determination which starts from the topocentric coordinates of the meteoroid trajectory. The method of obtaining the meteoroid's state vector is based on a larger set of perturbations, which are tracked backwards in time from the entry point of the meteoroid, to a point outside the Earth's sphere of influence. Our method is then applied to a bolide recorded within MOROI network, and the outcome is compared with the results obtained with previously published techniques. Finally, a forward and backward propagation in time of the meteoroid is presented using the described equations of motion, and fourth-order symplectic Neri integrator.

*Key words*: Celestial Mechanics – Meteors – Orbit determination – Numerical integration.

## 1. INTRODUCTION

Meteor monitoring devices are widespread worldwide. These recording tools range from optical and radio antennas, up to detections of meteoroid generated shock using infrasound arrays, and seismic detectors for larger events *e.g.* Brown *et al.* (2013). Among devices, CCD sensors are the most common tools to monitor the sky, and due to their availability, are used both by the professional and amateur community. The cameras range from narrow field, up to the whole sky, and used in combination of two or more (*i.e.* in the case of networks), can result in a meteor trajectory reconstruction.

The *Fireball Recovery and InterPlanetary Observation Network* (FRIPON), consisting now of more than 150 cameras, has been monitoring meteoroid entries since 2015, thereby allowing the characterization of their dynamical and physical properties (Colas *et al.*, 2020). Furthermore, by modeling the dark flight of the re-

[*] These authors contributed equally to this work

maining fragments, this can lead to meteorite recoveries (Gardiol *et al.*, 2021).

A similar approach was implemented in Romania since 2016 (Nedelcu *et al.*, 2018). Following the installation of a FRIPON camera in Bucharest, a first set of 3 cameras was deployed in Transylvania, thus starting the *Meteorites Orbits Reconstruction by Optical Imaging* network (MOROI). Now, the gradually increasing infrastructure in Romania consists of 16 stations, 7 of which are already integrated with the FRIPON international database*.

The MOROI cameras are based on Sony ICX445 sensor (Anghel *et al.*, 2019a; Colas *et al.*, 2020), which offers a resolution of 1.3 mp to monitor the local sky. The meteor detection procedure is operated by FreeTure open-source software (Audureau *et al.*, 2014). For calibrations, the software grabs a long exposure (5 seconds) *capture* every 10 minutes. These images are used to keep track of star positions in the image, and to measure their magnitude, thus calibrating the meteor's astrometry and photometry. In addition, the *captures* can also be used to perform local sky quality studies (Birlan *et al.*, 2021; Anghel *et al.*, 2019b). An increase in the number of cameras in a given area will result in an ample observation mesh, which will help to cross calibrate the stations, and ameliorate the uncertainty along the trajectory (Jeanne *et al.*, 2019). This output can be used to better identify meteor showers and forecast their activity as described by (Egal, 2020) and the references therein. As of 2021, the IAU *Meteor Data Center* (MDC)† contains 112 officially "established" meteor showers, connected with the past activity of the parent object. Many of these parent objects are just now being discovered by the minor planet surveys, or by the associations with the already discovered objects (Babadzhanov, 2010; Dumitru *et al.*, 2017, 2018). Moreover, the MDC contains 702 more showers on the working group (*i.e.* published in the literature), which are yet to be connected with parent objects.

New showers can arise from the activations of Near-Earth objects. These events can either be spotted directly (in a fortunate scenario) as presented by *e.g.* Marsset *et al.* (2019), or indirectly, as a new minor stream. Studying the latter is of uttermost importance as most of minor streams (as in the case of the Working group) cannot be immediately linked with the source object due to various reasons (*e.g.* low albedo, high phase angle, small size). Thus, a proper tracking of the stream's activity and dynamical evolution can impose better constrains on the orbital torus, along which the parent object can be discovered.

For this study, we present a method of orbit determination for a meteoroid entering the atmosphere. First, we start from the topocentric measurements of a trajectory and describe the perturbations involved in the near-Earth scenario. Next, we describe the methods to compute the apparent radiant and orbit and we apply

*`https://www.fripon.org/`

†`http://www.ta3.sk/IAUC22DB/MDC2007/index.php/` (accessed 24 April 2021)

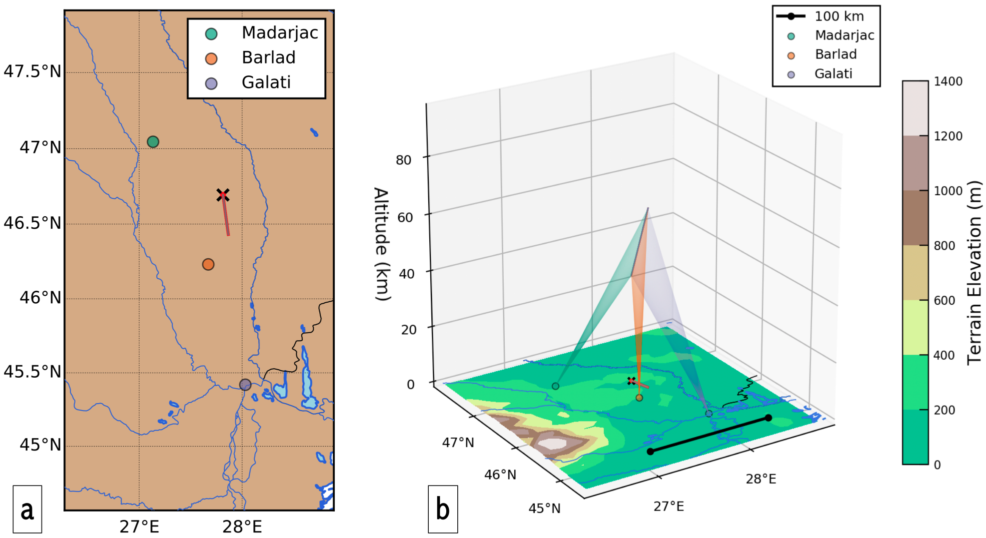


Fig. 1 – The 2D (a) and 3D (b) representations of the computed trajectory of the 20190502T214139_UT event recorded in the MOROI network. Both representations are based on cylindrical world map projections. The location of the stations, relief and altitude are also displayed. The red line and black cross mark the ground projections of the fireball and final point, respectively of the visible trajectory. The black segment (b) displays the computed length of 100 km at 45° latitude.

the computations for a meteor recorded in the MOROI network (Figure 1). Finally, the meteoroid orbit is numerically integrated with our developed model in order to identify their plausible source regions, which can eventually lead to the identification of their parent bodies.

## 2. METHOD OF ORBIT DETERMINATION

### 2.1. PATH TO PREATMOSPHERIC ORBIT

An analysis of meteor observations yields the azimuth and the inclination of the atmospheric trajectory (*i.e.* a topocentric radiant) of a meteor, its apparent velocity, and the coordinates of the origin of its visual path (Figure 1). The geometrical model presented by Ceplecha (1987), allows us to separate the space and time components of our measurements and to overcome the problem of temporal accuracy. The application of this method for MOROI network is described by Nedelcu *et al.* (2018).

The meteoroid moves in the field of action of various forces that are modeling its trajectory. The most important of these is the gravitational force, which comes mainly from the attraction of the Earth. To study the effect of the nonsphericity of the Earth's gravitational field on meteoroid motion involves the consideration of the theory of gravitational potential. In consequence, we considered the terms of the Earth's gravitational potential up to $c_{50}$ for zonal harmonics and $c_{33}$, $s_{33}$ for tesseral harmonics.

The other major perturbation for a meteoroid's motion near to the Earth (in our case about 200 km altitude over the Earth's surface) is the atmospheric drag. A significant number of studies is devoted to the problem of atmospheric drag. In this article we will consider the drag caused by the rotating atmosphere.

Another perturbation on the object is the effect of the solar and lunar attraction, which differ from each other only in quantity. The effect of the solar radiation pressure is another disturbance, which could produce secular variations in the orbit.

Other factors acting upon the motion of the meteoroid can be the effect of the Earth's magnetic field, the effect of the electrostatic field existing in the ionosphere and the effect of the radiation reflected from the Earth, etc. (Zieliński, 1968; Roy, 1988; Montenbruck, 2000; Szücs-Csillik, 2017; Clark and Wiegert, 2011). These factors produce minimal effects in our case.

Let us take a coordinate system $x$, $y$, $z$ with origin in Earth's center. We are considering perturbations due to the oblateness of Earth, to the atmospheric drag and to the luni-solar attraction. The differential equations of meteoroid motion in rectangular coordinates have the form:

$$\begin{aligned} \frac{d^2x}{dt^2} &= \frac{\partial U}{\partial x}, \\ \frac{d^2y}{dt^2} &= \frac{\partial U}{\partial y}, \\ \frac{d^2z}{dt^2} &= \frac{\partial U}{\partial z}, \end{aligned} \tag{1}$$

where

$$U = U_{00}+U_{20}+U_{22}+U_{30}+U_{31}+U_{32}+U_{33}+U_{40}+U_{50}+U_A+U_{RP}+U_{LS}, \tag{2}$$

and the particular terms are respectively

$$
\begin{aligned}
U_{00} &= \frac{\mu}{r}, \qquad (3)\\
U_{20} &= \frac{1}{2}\mu R^2 c_{20}\cdot\left(\frac{3z^2}{r^5}-\frac{1}{r^3}\right),\\
U_{22} &= 3\mu R^2\left[\left(\frac{x^2-y^2}{r^5}c_{22}+\frac{2xy}{r^5}s_{22}\right)\cos 2s+\right.\\
&+\left.\left(\frac{2xy}{r^5}c_{22}-\frac{x^2-y^2}{r^5}s_{22}\right)\sin 2s\right]\\
U_{30} &= \frac{1}{2}\mu R^3 c_{30}\cdot\left(\frac{5z^3}{r^7}-\frac{2z}{r^5}\right),\\
U_{31} &= \frac{3}{2}\mu R^3\left[\left(\left(\frac{5xz^2}{r^7}-\frac{x}{r^5}\right)c_{31}+\left(\frac{5yz^2}{r^7}-\frac{y}{r^5}\right)s_{31}\right)\cos s+\right.\\
&+\left.\left(\left(\frac{5yz^2}{r^7}-\frac{y}{r^5}\right)c_{31}-\left(\frac{5xz^2}{r^7}-\frac{x}{r^5}\right)s_{31}\right)\sin s\right],\\
U_{32} &= 15\mu R^3\left[\left(\left(\frac{(x^2-y^2)\cdot z}{r^7}\right)c_{32}+\left(\frac{2xyz}{r^7}\right)s_{32}\right)\cos 2s+\right.\\
&+\left.\left(\left(\frac{2xyz}{r^7}\right)c_{32}-\left(\frac{(x^2-y^2)\cdot z}{r^7}\right)s_{32}\right)\sin 2s\right],\\
U_{33} &= 15\mu R^3\left[\left(\left(\frac{x\cdot(x^2-3y^2)\cdot z}{r^7}\right)c_{33}+\left(\frac{y\cdot(3x^2-y^2)}{r^7}\right)s_{33}\right)\cos 3s+\right.\\
&+\left.\left(\left(\frac{y\cdot(3x^2-y^2)}{r^7}\right)c_{33}-\left(\frac{x(x^2-3y^2)\cdot z}{r^7}\right)s_{33}\right)\sin 3s\right],\\
U_{40} &= \frac{1}{8}\mu R^4 c_{40}\cdot\left(\frac{35z^4}{r^9}-\frac{30z^2}{r^7}+\frac{3}{r^5}\right),\\
U_{50} &= \frac{1}{8}\mu R^5 c_{50}\cdot\left(\frac{63z^5}{r^{11}}-\frac{70z^3}{r^9}+\frac{15z}{r^7}\right),\\
U_A &= -\frac{1}{2}\frac{\rho C_D A}{m}v_r\overline{v_r},\\
U_{RP} &= p\cdot\frac{A}{m},\\
U_{LS} &= \frac{\mu'}{r'}\cdot\left(1+\frac{r^2}{2r'^2}\cdot(3\cos(2\psi-1))\right)+\frac{\mu''}{r''}\cdot\left(1+\frac{r^2}{2r''^2}\cdot(3\cos(2\psi-1))\right),
\end{aligned}
$$

where $\mu$ is the gravity constant $G$ multiplied by the sum of Sun's and Jupiter's mass (in our case $\mu = 0.00029\ AU^3/days^2$), $r$ is the distance from the center of mass to the meteoroid, $R$ is the equatorial radius of the Earth ($R = 0.000042\ AU$), $c_{20} =$

$-1082.4$, $c_{22}=0.75$, $s_{22}=-0.61$, $c_{30}=2.57$, $c_{31}=0.87$, $s_{31}=-0.27$, $c_{32}=0.08$, $s_{32}=-0.09$, $c_{33}=-0.07$, $s_{33}=0.129$, $c_{40}=2.01$, $c_{50}=0.07$ are zonal and tesseral coefficients, $s$ is the argument of latitude, and $\rho$ is the atmospheric density, $C_D$ is the drag coefficient, $A/m$ is the cross section to the mass of meteoroid ratio, $v_r$ is the meteoroid velocity vector relative to atmosphere, and $p$ is the solar light pressure at the distance of one AU, $\mu', \mu''$ are the masses of the disturbing bodies (Moon, Sun) multiplied by the gravitational constant, $r', r''$ are the radius vectors of the disturbing bodies, $\psi$ is the Sun-Moon distance angle as seen from the Earth.

Let us consider the simple exponential atmospheric model

$$\rho = \rho_p \exp\left(\frac{r_p - r}{H}\right), \tag{4}$$

where $\rho_p$ is the density at initial perigee point, obtained via the the NRLMSISE-00 model (Picone *et al.*, 2002), $r_p$ is the initial distance of the meteoroid from Earth's surface and $H$ is the scale height. Let us denote $B = \frac{m}{C_D A}$ the Ballistic coefficient, and we assume that the atmosphere rotates at the same angular speed as the Earth. Then, the relative velocity vector is

$$\mathbf{v_r} = \mathbf{v} - \omega \times \mathbf{r}, \tag{5}$$

where $\omega$ is the initial rotation vector of the Earth around the $z$ axis with $\omega_e = 7.29 \cdot 10^{-5}$ rad/sec. The relative velocity vector is $\mathbf{v_r} = (v_x + \omega_e y, v_y - \omega_e x, v_z)$.

### 2.2. INITIAL CONDITIONS

Following the equations presented in section 2, from the entry point up to $\approx$10 lunar distances, this yields an initial heliocentric state vector of the meteoroid. Next, the aim is to translate the rectangular real-time coordinates into orbital (Keplerian) elements. These are used to uniquely identify a specific orbit with a set of six parameters:

- $a$ [AU] – the semi-major axis;
- $i$ [deg] – the orbital inclination;
- $e$ – the eccentricity;
- $\omega$ [deg] – the argument of perihelion;
- $\Omega$ [deg] – the longitude of ascending node;
- $M$ [deg] – the mean anomaly or $v$ [deg] - the true anomaly.

Semimajor axis $a$ is used to compute the total energy of the orbit and together with eccentricity $e$, allows us to compute the angular momentum (Figure 2). The meteoroid's angular position in the orbit at a given epoch is defined by the true anomaly $v$. For that reason, $a, e, v$ give information about the size and shape of the meteoroid's orbit, and its location in the orbital plane. The inclination $i$, the longitude of the ascending node $\Omega$ and the argument of periapsis $\omega$ define the orientation of the orbit in three-dimensional space (Seidelmann, 1992; Vallado, 2013).

Moreover, the argument of latitude is $u = \omega + v$, measured in the orbital plane from the ascending node to the radius vector $\mathbf{r}$, and the true longitude of the meteoroid at epoch is identified as $l = \Omega + \omega + v$. These two new orbital elements can be used in place of the true anomaly $v$ at epoch.

Motion in the solar system is not restricted to a single orbital plane and for that reason we consider the Cartesian state vector $(\mathbf{r}, \mathbf{v})$, because it entirely defines the meteoroid's orbit. Let us mention, as previously marked, that the classical orbital elements $(a, e, i, \Omega, \omega, v)$ are useful in visualizing, in our case, the meteoroid's orbit. Figure 2 shows the relationship between the orbital plane coordinate system and the reference plane system.

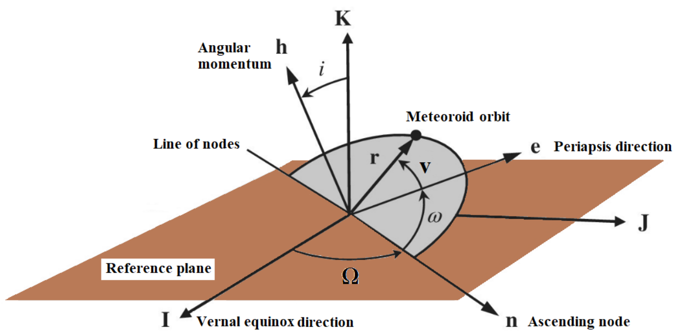


Fig. 2 – Orbital motion with respect to the reference plane in space.

The orbital plane is in the perifocal coordinate system (PQW). Perifocal word states that the main axis $x_{PQW}$ points from the focus to the pericenter (perihelion) direction, the $y_{PQW}$ axis is in the direction of the meteoroid's motion, and the $z_{PQW}$ is perpendicular to the orbital plane along the angular momentum. Let us mention that for the definition of a coordinate system in a three dimensional space, one needs only to specify the direction of one of the axes, and the orientation of one of the other axes in the plane perpendicular to this direction. The third axis follows automatically in order to complete a right-handed orthogonal set.

Our reference coordinate system is the *Earth-centered inertial* (ECI) coordinate system, where the coordinates are defined as the distance from the origin along the three orthogonal (mutually perpendicular) axes.

The $x_{ECI}$ axis points in the direction of the vernal equinox, the $z_{ECI}$ axis runs along the Earth's rotational axis pointing North, the $y_{ECI}$ axis completes the right-handed orthogonal system. For example, when considering the motion of the meteoroid around the Sun, it is common to use heliocentric coordinate system, where the reference plane is the plane of the ecliptic (Earth's orbit) and the reference line is in the direction of the vernal equinox.

In orbital determination studies around the Earth it is necessary to transform from one coordinate system to another. Therefore, as a first step we use the given orbital elements to develop a state vector $(\mathbf{r}_{PQW}, \mathbf{v}_{PQW})$ expressed in the *perifocal coordinate system* (PQW).

The polar coordinates in the plane of the orbit are the heliocentric distance $r$ and the true anomaly $v$, and the $z$-component of the meteoroid is necessarily zero. Therefore, the position vector is given by

$$\mathbf{r}_{PQW}(x_{PQW}, y_{PQW}, z_{PQW}) = \begin{bmatrix} r \cdot \cos v \\ r \cdot \sin v \\ 0 \end{bmatrix}, \tag{6}$$

where the radius vector and the true anomaly are calculated from the following equations

$$\begin{aligned} r &= a \cdot (1 - e \cdot \cos E), \\ \tan v &= \frac{\sqrt{1-e^2} \cdot \sin E}{\cos E - e}. \end{aligned} \tag{7}$$

We note that using simple iterative techniques the numerical solution of Kepler's equation gives the eccentric anomaly $E$:

$$E_{i+1} = M + e \cdot \sin E_i, \qquad i = 0, 1, \ldots, \tag{8}$$

with $E_0 = M$ as a first approximation.

We can also find the radial $\dot{x}$ and transverse $\dot{y}$ components of the velocity vector in PQW coordinate system by taking time derivatives of the expressions for $x$ and $y$. This gives

$$\mathbf{v}_{PQW}(\dot{x}_{PQW}, \dot{y}_{PQW}, \dot{z}_{PQW}) = \begin{bmatrix} -\sqrt{\frac{\mu}{p}} \cdot \sin v \\ \sqrt{\frac{\mu}{p}} \cdot (e + \cos v) \\ 0 \end{bmatrix}, \tag{9}$$

where the semi-latus rectus is $p = a \cdot (1 - e^2)$. Let us mention that $\mu$ is the standard gravitational parameter. In our case, $\mu = G \cdot (M_S + M_J)$, introduced above, in Eq. (3), where $M_S$ and $M_J$ are the masses of Sun and Jupiter, respectively.

Obviously, the coordinates in one system can be expressed in terms of the other by means of a series of three rotations about the axes.

In the second step, we transform from the perifocal coordinate system (PQW) to the general (ECI) reference system.

Firstly, with a rotation about the $z$ axis through the angle of the argument of perihelion $\omega$, so that the $x$ axis coincides with the line of nodes.

Secondly, a rotation about the $x$ axis through the angle of the inclination $i$, so that the two planes become the same.

Thirdly, a rotation about the $z$ axis through the angle of the longitude of the ascending node $\Omega$. We can write these transformations by three $3 \times 3$ rotation matrices, denoted by $\mathbf{R3}(\omega)$, $\mathbf{R1}(i)$, $\mathbf{R3}(\Omega)$.

$$\mathbf{R3}(\omega) = \begin{bmatrix} \cos\omega & \sin\omega & 0 \\ -\sin\omega & \cos\omega & 0 \\ 0 & 0 & 1 \end{bmatrix},$$

$$\mathbf{R1}(i) = \begin{bmatrix} 1 & 0 & 0 \\ 0 & \cos i & \sin i \\ 0 & -\sin i & \cos i \end{bmatrix},$$

$$\mathbf{R3}(\Omega) = \begin{bmatrix} \cos\Omega & \sin\Omega & 0 \\ -\sin\Omega & \cos\Omega & 0 \\ 0 & 0 & 1 \end{bmatrix}.$$

Therefore, the transformations from the PQW to the ECI coordinate system are

$$\mathbf{R} = \mathbf{R3}(\Omega)^{-1} \cdot \mathbf{R1}(i)^{-1} \cdot \mathbf{R3}(\omega)^{-1},$$

$$\begin{aligned} \mathbf{r}_{ECI} &= \mathbf{R} \cdot \mathbf{r}_{PQW}, \\ \mathbf{v}_{ECI} &= \mathbf{R} \cdot \mathbf{v}_{PQW}, \end{aligned} \tag{10}$$

where $\mathbf{R3}^{-1}$ is the inverse of the matrix $\mathbf{R3}$, and so forth. We note that because all rotation matrices are orthogonal, the inverse of each matrix is equal to its transpose. These steps allow us to compute the impact location of an object with known orbit.

Converting the state vector into the unit vector counterpart $(\xi, \eta, \zeta)$, and using a spherical representation as

$$\begin{aligned} d_{radiant} &= \sqrt{\xi^2 + \eta^2 + \zeta^2} \\ \alpha_{radiant} &= \tan^{-1} \frac{\eta}{\xi} \\ \delta_{radiant} &= \tan^{-1} \frac{\sqrt{\xi^2 + \eta^2}}{\zeta}, \end{aligned} \tag{11}$$

the apparent sky coordinates of the radiant are obtained.

*Table 1*

Fireball radiant and heliocentric orbit

| | | |
|---|---|---|
| Topocentric radiant | | |
| Azimuth | $172.215^\circ$ | |
| Elevation | $40.829^\circ$ | |
| Beginning Height | $63.80$ km | |
| Beginning Latitude | $46.43^\circ$ | |
| Beginning Longitude | $27.87^\circ$ | |
| Apparent radiant (J2000) | | |
| Right ascension | $219.37^\circ$ | |
| Declination | $-2.12^\circ$ | |
| $V_\infty$ | $25.118 \pm 0.3$ km $s^{-1}$ | |
| Orbital elements (J2000) | Meteor Toolkit | this work |
| a, AU | 2.8271 | 2.7391 |
| e | 0.7775 | 0.7594 |
| i, $^\circ$ | 6.8080 | 8.2971 |
| $\Omega$, $^\circ$ | 41.9739 | 41.9385 |
| $\omega$, $^\circ$ | 261.9076 | 258.5741 |
| M (at epoch), $^\circ$ | 350.2362 | 350.4550 |
| Epoch | 29 Apr 2019 21:41:39 UT | |

## 3. RESULTS

### 3.1. THE ORBIT

The relations detailed in section 2 were applied to the 2 May 2019 bolide, recorded in the MOROI network at 23:41:39 local time (21 UT). The fireball (20190502T214139_UT), detected from Barlad, Galati and Madarjac (ROVS01, ROGL01, ROIS01 now, within MOROI/FRIPON) allowed trajectory computations, thus obtaining the geocentric coordinates of the object and the apparent radiant (Figure 3). Next, the conversion into topocentric coordinates resulted in longitude, latitude and height above ground of the beginning and final point of the atmospheric path (see Figure 1).

An important aspect of this article is to also describe steps for deriving a heliocentric meteoroid orbit. Furthermore, we compared our method with the results obtained via the Meteor Toolkit (MT) program (v3.5). Details about the functionality of the software can be found in the manuscript by Dmitriev *et al.* (2015). The resulted values for 20190502T214139_UT orbit comparison, along with additional details are presented in Table 1. Also, the representation of both orbits, along with the state of the Solar System are in Figure 4.

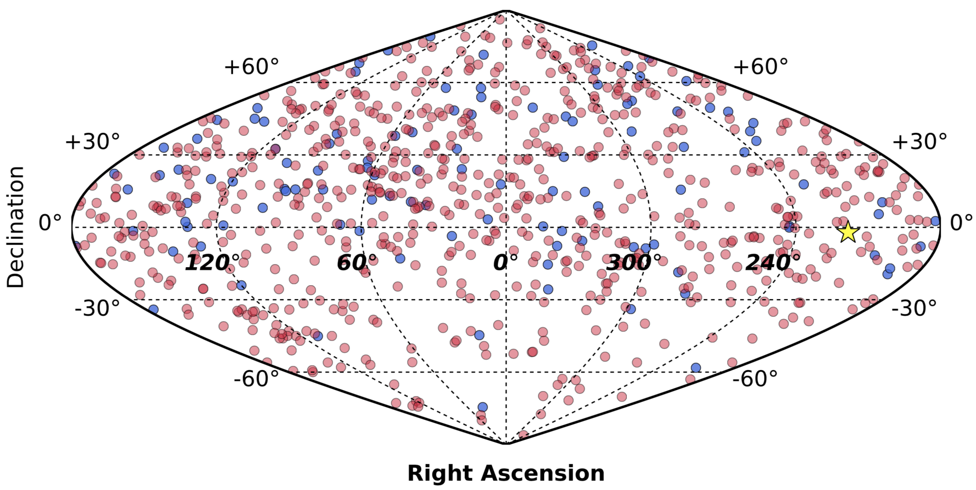


Fig. 3 – The meteor showers listed in the IAU Meteor Data Center represented in a Sanson–Flamsteed projection. The established showers are represented by the blue circles, while the showers which appear on the working list are represented by red dots. The apparent radiant of the 20190502T214139_UT event is marked by the yellow star.

3.2. NUMERICAL INTEGRATION

During the close approaches to the Earth, the meteoroid's orbit is continuously perturbed by the planet's gravity (Vida *et al.*, 2020). Thus, a numerical integrator was implemented to simulate the long term gravitational dynamics of a meteoroid.

For this, two numerical integration methods were analyzed: a non-separable fourth-order symplectic integrator (Csillik, 2004; Szücs-Csillik, 2010), and the Runge-Kutta-Fehlberg integrator. As is generally known, the numerical integration methods which inherit the symplecticity of a differential equations tend to better approximate the trajectory of a symplectic differential equation.

Moreover, the fourth-order symplectic integrator scheme is time reversible because it is symmetric. It is common knowledge that the time reversibility is important, it ensures the two first integrals, *i.e.* the conservation of energy and the area preserving. For example, in the Runge-Kutta forth-order method, different deriva-

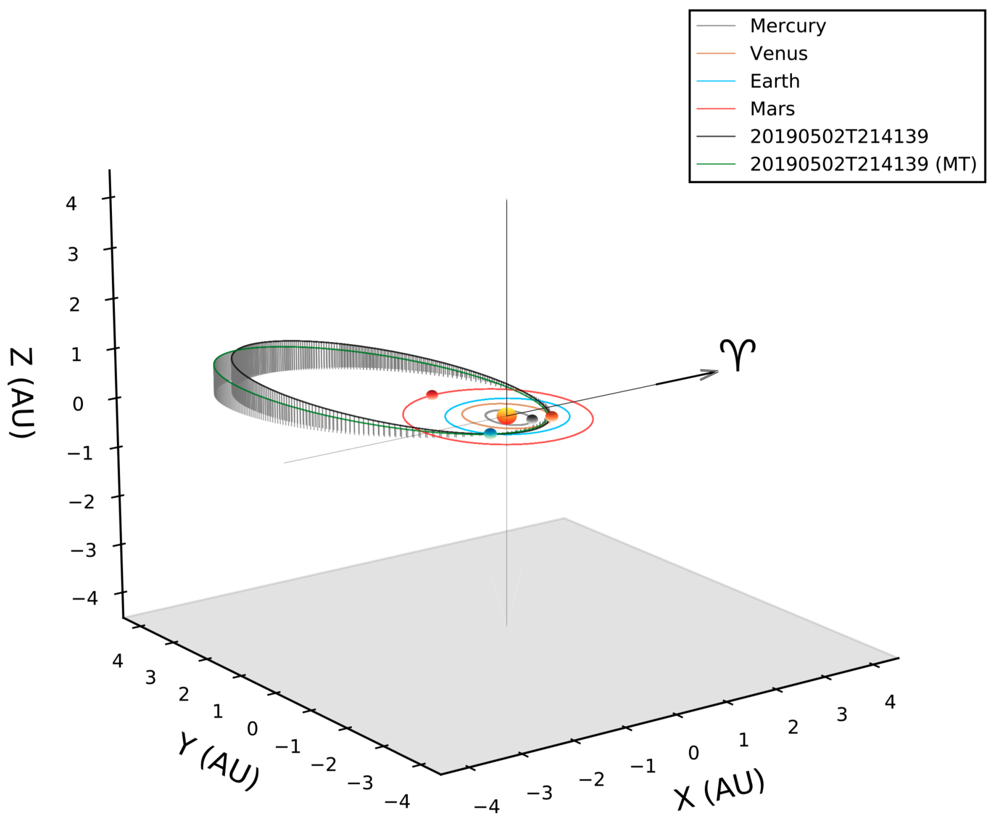


Fig. 4 – The orbit of the meteoroid represented in 3D heliocentric rectangular coordinates, computed for J2000.

tives are used, which are evaluated at different times. So, the forward and backward steps would not match exactly. Obviously, the difference is small, but it is enough to prevent the fourth order Runge-Kutta integrator from being exactly time reversible.

In our numerical example we require integration in the reverse-time direction also. Therefore, we are interested to simulate the reverse-time system, and if we use the fourth-order symplectic scheme to integrate forward in time, reversing the sign of the time-step of the same integrator to return to initial time $t = 0$, we will arrive at our starting point. However, in the case of fourth-order Runge-Kutta integrator, the scheme leads to an approximately close point to the starting point.

Particularly, the fourth-order Neri (Neri, 1987) symplectic integrator is a member of the family of symplectic integrators for solving an initial value problem (Csillik, 2004). The fourth-order Neri symplectic integrator is defined by the formulae:

$$\begin{aligned} \frac{d\mathbf{z}}{dt} &= D_H(\mathbf{z}) = \{\mathbf{z}, H\}, \\ \mathbf{z}(t_0) &= z_0, \end{aligned} \tag{12}$$

where $H = T + V$ is the Hamiltonian of the system. The exact time evolution of $\mathbf{z}(t)$ from $t = 0$ to $t = \tau$ is given by

$$\mathbf{z}(\tau) = \exp(\tau D_H) \cdot \mathbf{z}(0) = \exp(\tau \cdot (D_T + D_V)) \cdot \mathbf{z}(0). \tag{13}$$

The mapping from $z = z(0)$ to $z' = z(\tau)$ would be

$$\mathbf{z}' = \prod_{i=1}^{n} [\exp(\tau \cdot (D_T + D_V)] \cdot \mathbf{z}, \tag{14}$$

where $\mathbf{z} = (\mathbf{q}, \mathbf{p})$, $\mathbf{q} = (q_x, q_y, q_z)$ are the generalized coordinates, $\mathbf{p} = (p_x, p_y, p_z)$ are the conjugated generalized momenta, and $(c_i, d_i)$, $i = \overline{1,n}$ is a set of real numbers. Explicitly,

$$\begin{aligned} q_i &= q_{i-1} + \tau c_i \cdot \left(\frac{\partial T}{\partial \mathbf{p}}\right)_{\mathbf{p}=p_{i-1}}, \quad i = \overline{1,n}, \\ p_i &= p_{i-1} + \tau d_i \cdot \left(\frac{\partial V}{\partial \mathbf{q}}\right)_{\mathbf{q}=q_i}, \end{aligned} \tag{15}$$

where

$$\begin{aligned} c_1 = c_4 &= \frac{1}{2 - 2^{\frac{1}{3}}}, \qquad c_2 = c_3 = \frac{1 - 2^{\frac{1}{3}}}{2 - 2^{\frac{1}{3}}}, \\ d_1 = d_3 &= \frac{1}{2 - 2^{\frac{1}{3}}}, \qquad d_2 = -\frac{2^{\frac{1}{3}}}{2 - 2^{\frac{1}{3}}}, \qquad d_4 = 0. \end{aligned} \tag{16}$$

The reverse-time symplectic scheme is slightly different from the Eqs. (15) and one can find it simply by changing the sign of the time, $\tau$.

The forward and backward simulations of the meteoroid orbit for the 2019 0502T214139_UT event are presented in Figure 5, the initial conditions in ECI coordinate system, using Eq. (10), at $t = 0$ are $q_x(0) = -0.7496$, $p_x(0) = 0.0211$, $q_y(0) = -0.6735$, $p_y(0) = -0.0055$, $q_z(0) = 2.3436 \cdot 10^{-6}$, $p_z(0) = -3.0701 \cdot 10^{-8}$, stepsize $= 0.1$.

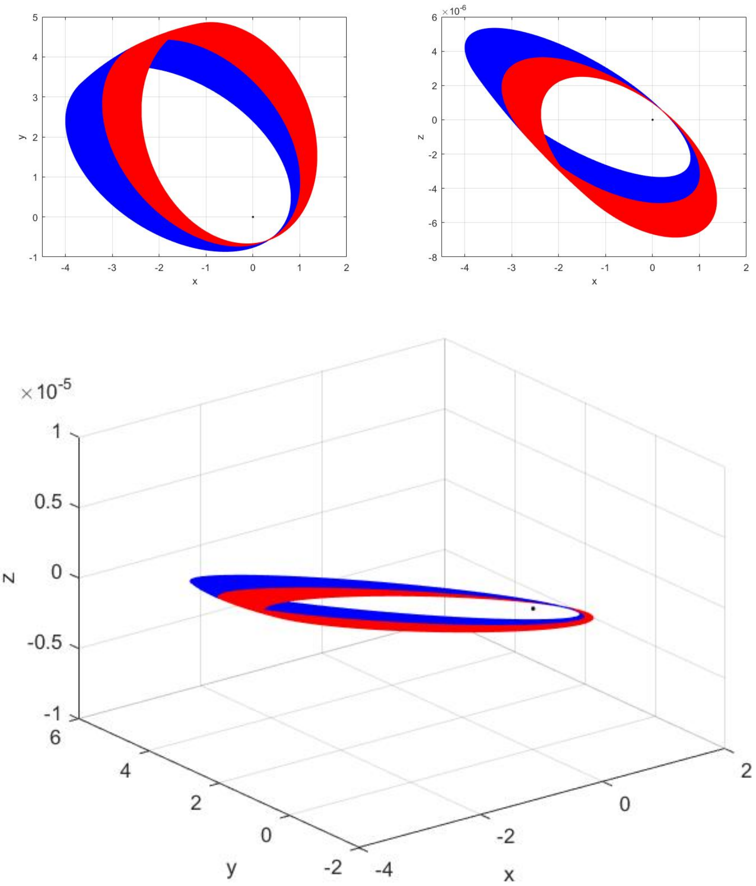


Fig. 5 – Perturbed meteoroid orbit integrated with the fourth-order symplectic Neri integrator for a long-time period of time (200000 years) in forward (red) and in backward (blue) directions.

In comparison, using the Runge-Kutta-Fehlberg forth-order integrator with the same initial conditions for a short-period of time (200 year) in forward (red) and backward (blue) lines, lead to Figure 6.

As illustrated in the last figures, the symplectic integrator is much more effective, faster, and with lower errors than the Runge-Kutta-Fehlberg integrator.

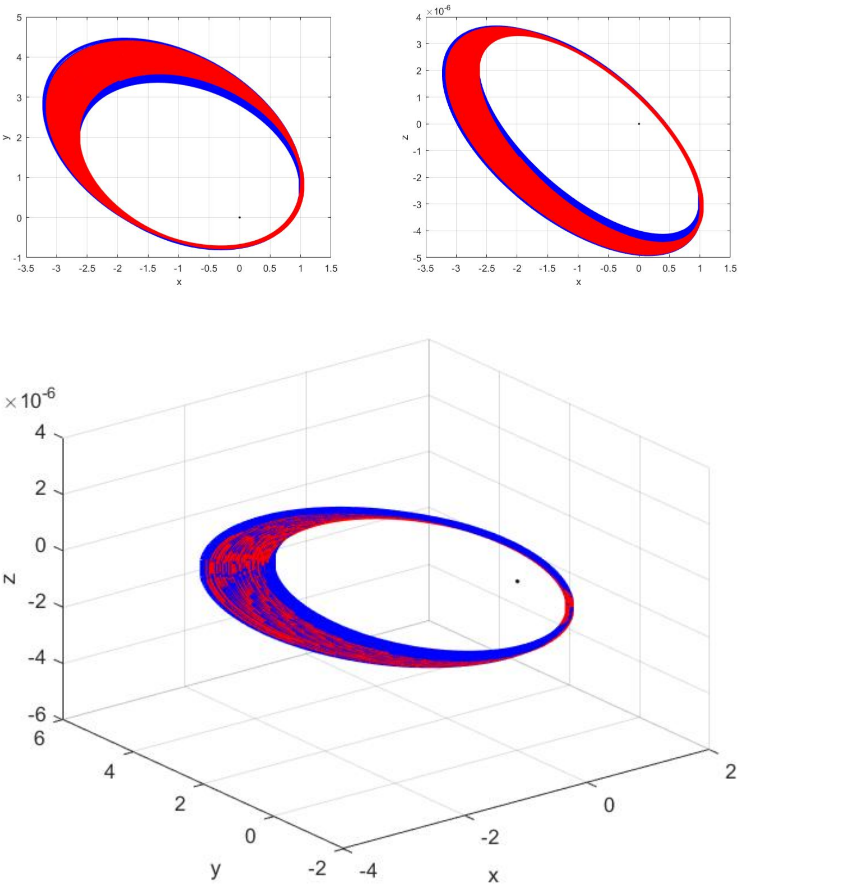


Fig. 6 – Perturbed meteoroid orbit integrated with the Runge-Kutta-Fehlberg forth-order integrator for a short-time period of time (200 years) in forward (red) and in backward (blue) directions.

As mentioned before, knowing the classical orbital elements one can describe the meteoroid's trajectory (see Table 1). In our case, the orbital size defined by the semimajor axis $a$ shows an orbit between Mars and Jupiter. The orbital shape is defined by its eccentricity $e$, which indicates an elliptic orbit. The inclination $i$ describes the tilt of the orbital plane with respect to the fundamental plane. For our case, the orbital plane is close to the ecliptic plane and the meteoroid is in direct orbit (see Figure 5). The right ascension of the ascending node, $\Omega$ is used to describe the orbital orientation with respect to the principal (vernal equinox) direction. This rotation of the orbital plane, gives us the swivel of the orbit. In our case the meteoroid moves in the orbital plane in the same direction as the Earth, on the ecliptic. The argument of perigee, $\omega$, is the angle measured in the direction of the meteoroid's motion from the ascending node to the pericentre. It gives us the orientation of the orbit within the orbital plane. Finally, the meteoroid's location in the orbit is represented by the true anomaly, $v$, which is the angle along the orbital path from perigee to the spacecraft's position. Let us mention, that only the true anomaly changes with time as the meteoroid moves in its orbit.

## 4. SUMMARY AND CONCLUSIONS

The meteoroid's differential equations are presented combining the effects of the nonsphericity of the Earth's gravitational field, the effect of the atmospheric drag, and the effect of the solar and lunar attraction. These equations of motion are solved numerically including the terms of the Earth's gravitational potential up to $c_{50}$ for zonal harmonics and $c_{33}$, $s_{33}$ for tesseral harmonics. These were used to compute the initial state of the meteoroid. For the initial conditions conversion, we completely described and wrote a Matlab code of the transformation from the orbital elements of the meteoroid to the ECI reference coordinate system (Eq. 10).

For the studied bolide, the initial orbital state vector obtained with our method, differs slightly ($< .1\%$) from the results obtained via the Meteor Toolkit software. Taking into account the larger number of perturbing forces, we consider our methods to be a better approximation of the meteoroid's orbit. Moreover, to integrate the perturbed motion of the meteoroid (Eqs. 1, 2, 3) forward and backward in time, we developed a Matlab code using the fourth-order symplectic Neri schema (based on Eqs. 15, 16).

Our goal was to build and model a high precision meteoroid orbit determination explained in details, a basic article that can be used be anyone interested in trajectory calculation of meteoroids.

A future work will include a larger data set, focusing on individual meteor streams, to better understand the impact of each perturbatory component in the dynamical evolution of meteoroids.

*Acknowledgements.* SA, ISC and DAN contribution is partially supported by a grant of the Romanian Ministry of Research and Innovation, CCCDI - UEFISCDI, project number PN-III-P1-1.2-PCCDI-2017-0226/16PCCDI/2018 , within PNCDI III. The work of IB and MB was supported by a grant of the Ministry of Research, Innovation and Digitization, CNCS/CCCDI – UEFISCDI, project number PN-III-P1-1.1-PD-2019-0784, within PNCDI III.

Anghel, S. and Szücs-Csillik, I. acknowledge the Europlanet 2024 RI project funded by the European Union's Horizon 2020 Research and Innovation Programme (Grant agreement No. 871149). We would like to take this opportunity to acknowledge the time and effort devoted by reviewer to improving the quality of this manuscript.

## REFERENCES


Anghel, S., Birlan, M., Nedelcu, D. A., Boaca, I.: 2019a, *Rom. Astron. J.* **29**, 189.

Anghel, S., Birlan, M., Nedelcu, D. A., Boaca, I.: 2019b, *EPSC-DPS JointMeeting* **2019**, EPSC, DPS2019, 1758.

Audureau, Y., Marmo, C., Bouley, S, *et al.*.: 2014, *Proceedings of the International Meteor Conference*, Giron, France, 18-21 September 2014, pp. 39.

Babadzhanov, P.B.: 2003, *A&A* **397**, 319.

Birlan, M. *et al.*: 2021, *RoAJ* **31**, 41.

Brown, P., Assink, J., Astiz, L. *et al.*: 2013, *Nature* **503**, 238.

Ceplecha, Z.: 1987, *Bulletin of the Astronomical Institute of Czechoslovakia* **38**, 222.

Clark, D. L., Wiegert, P. A.: 2011, *Meteoritics & Planetary Science* **46**,1217.

Colas, F. *et al.*: 2020, *Astronomy & Astrophysics* **644**, A53.

Csillik, I.: 2004, *Technische Mechanik* **24**, 67.

Dmitriev, V., Lupovka, V., Gritsevich, M.: 2015, *Planetary and Space Science* **117**, 223.

Dumitru, B. A.; Birlan, M.; Popescu, M.; Nedelcu, D. A.: 2017, *Astronomy & Astrophysics* **607**, id. A5.

Dumitru, B. A.; Birlan, M.; Nedelcu, D. A.: 2018, *Romanian Astronomical Journal* **28**, 167.

Egal, A.: 2020, *Planetary and Space Science* **185**, id. 104895.

Gardiol, *et al.*: 2021, *MNRAS* **501**, 1215.

Jeanne, S. *et al.*: 2019, *Astronomy & Astrophysics* **627**, id. A78.

Marsset, M. DeMeo, F., Sonka, A., Birlan, M., Polishook, D., Burt, B., Binzel, R. P., Bus, S. J., Thomas, C.: 2019, *The Astrophysical Journal Letters* **882**, id. L2.

Montenbruck, O., Gill, E.: 2000, *Satellite Orbits, Models, Methods and Applications*, Springer-Verlag, Berlin.

Nedelcu, D. A., Birlan, M., Turcu, V. *et al.*: 2018, *Romanian Astron. J.* **28**, 57.

Neri, F.: 1987, *Dept. of Physics, University of Maryland*.

Roy, A.E.: 1988, *Orbital motion*, Bristol, England UK.

Picone, J. M., Hedin, A. E., Drob, D. P., Aikin, A. C.: 2002, *Journal of Geophysical Research (Space Physics)* **107**, id. 1468.

Seidelmann, P.: 1992, *E*xplanatory Supplement to the Astronomical Almanac, University Science Books, Mill Valley, CA.

Szücs-Csillik, I.: 2010, *Romanian Astronomical Journal* **20**, 49.

Szücs-Csillik, I.: 2017, *Romanian Astronomical Journal* **27**, 241.

Vallado, D.A.: 2013, *Fundamentals of Astrodynamics and Applications*, 4th edition, Microcosm Press, Hawthorne, CA.

Vida, D., Gural, P.S., Brown, P.G., Campbell-Brown, M., Wiegert, P.: 2020, *MNRAS* **491**, 2688.

Zieliński, J. B.: 1968, *Prace Naukowe Geodezja*, **1**, 7.


*Received on 25 May 2021*